

## Chapter 25

# What Seismic Risk Do We Design for When We Design Buildings?



Iunio Iervolino

**Abstract** This paper discusses two issues related to the seismic performance of code-conforming structures from the probabilistic standpoint: (i) the risk structures are implicitly exposed to when designed via state-of-the-art codes; (ii) which earthquake scenarios are expected to erode the portion of safety margins determined by elastic seismic actions for these structures. Both issues are addressed using recent research results referring to Italy.

Regarding (i), during the last few years, the Italian earthquake engineering community is putting effort to assess the seismic risk of structures designed according to the code currently enforced in the country, which has extended similarities with Eurocode 8. For the scope of the project, five structural typologies were designed according to standard practice at five sites, spanning a wide range of seismic hazard levels. The seismic risk assessment follows the principles of performance-based earthquake engineering, integrating probabilistic hazard and vulnerability, to get the annual failure rates. Results, although not fully consolidated yet, show risk increasing with hazard and uneven seismic reliability across typologies.

With regard to (ii) it is discussed that, in the case of elastic design actions based on probabilistic hazard analysis (i.e., uniform hazard spectra), exceedance of spectral ordinates can be likely-to-very-likely to happen in the epicentral area of earthquakes, which occur relatively frequently over a country such as Italy. Although this can be intuitive, it means that design spectra, by definition, do not necessarily determine (elastic) design actions that are conservative for earthquakes occurring close to the construction site. In other words, for these scenarios protection is essentially warranted by the rarity with which it is expected they occur close to the structure

---

This manuscript is largely based on the papers by Iervolino et al. (2017) and Iervolino and Giorgio (2017)

I. Iervolino (✉)

Dipartimento di Strutture per l'Ingegneria e l'Architettura, Università degli Studi di Napoli Federico II, Naples, Italy

e-mail: [iunio.iervolino@unina.it](mailto:iunio.iervolino@unina.it)

and further safety margins implicit to earthquake-resistant design (i.e., those discussed in the first part).

## 25.1 Introduction

In the current state-of-the-art seismic codes (e.g., the Italian building code, CS.LL. PP. 2008, NTC08 hereafter, similar to Eurocode 8 or EC8, CEN 2004) structural performance, with respect to violation of given limit states (*failure* hereafter), must be verified for levels of ground motions associated with specific exceedance return period ( $T_r$ ) at the building site. In case of ordinary structures, for example, safety verifications for *life-safety* and *collapse-prevention* limit states are required against ground motion levels that are exceeded on average once every 475 and 975 years (probabilities of exceedance of 10% and 5% in 50 years), respectively.<sup>1</sup> In such a design practice, if failure were to always occur for intensities larger than those considered during design, and never did occur for intensities lower than the design one, then the risk of failure (i.e., the seismic risk) would be equal to the exceedance rate of the design intensity, that is the reciprocal of the return period. However, thanks to code requirements, it is generally expected that the seismic risk of failure is smaller than that of exceedance of the design ground motion. On the other hand, these further safety margins are neither explicitly controlled nor quantified, which means that the resulting seismic risk, that is the rate of earthquakes causing failure of code-conforming structures, is implicit to structural design.<sup>2</sup>

When modern codes are concerned, a rational safety goal might be that designing two different structures for the seismic intensity with the same exceedance return period brings comparable seismic risk. For example, two structures belonging to the same structural typology, with the same use, designed in different sites, or different structural typologies designed for the same limit state at the same site. However, because there's no probabilistic control beyond exceedance of elastic design actions, it is not granted neither that the same exceedance probability determines the seismic risk nor that such a risk is necessarily acceptable.

The research work discussed herein intends to shed some light on what is the seismic risk of (Italian) code-conforming structures designed for seismic actions based on probabilistic seismic hazard analysis and, given that failure is allowed by state-of-the-art codes, in which earthquakes it is more likely. To this aim, the rest of the manuscript is divided in two parts. In the first one, the results of a large research project attempting to assess the implicit-by-design seismic risk of standard code-conforming buildings, is discussed. For the scope of the project, five structural

---

<sup>1</sup>In EC8 the same actions are used for the limit states identified as *significant damage* and *near collapse*, respectively.

<sup>2</sup>Other quantities such as material design characteristics or design loads originate from probabilistic considerations, yet their reflection of the global safety margins of the structure is structure-specific and is not explicitly controlled.

typologies were designed according to the most recent seismic code and standard practice at five sites, spanning a wide range of design hazard from low- to high-seismicity. These structures are also finely modeled to capture dynamically their three-dimensional non-linear behavior during earthquakes. The assessment of their risk follows the principles of performance-based earthquake engineering integrating probabilistic hazard and vulnerability, to get the annual failure rates.

Once the rate of earthquakes causing violation of the performance levels of interest is assessed, it may be interesting to change the perspective and to look, from the seismic hazard side, what are the earthquake scenarios (i.e., magnitude and location with respect to the construction site) for which design intensity is exceeded with high probability. To this aim, it is discussed that, in the case of elastic actions based on probabilistic hazard analysis (i.e., uniform hazard spectra), exceedance of spectral ordinates can be likely-to-very-likely to happen in the epicentral area of earthquakes, which are not necessarily of extreme magnitude. Although this can be intuitive, it means that design spectra do not necessarily determine (elastic) design actions conservative for moderate-to-high magnitude earthquakes (i.e., those occurring every few years over Italy) in case they occur close to the construction site. In other words, for these scenarios protection is basically warranted by the rarity with which it is expected they occur close to the structure or, in case of occurrence, by further safety margins implicit to earthquake-resistant design (i.e., those not explicitly controlled that are discussed in the first part).

## 25.2 The RINTC 2015–2017 Project

To quantitatively address the seismic risk code-conforming design implicitly exposes structures to, a large research project is ongoing in Italy. This project, named *Rischio Implicito di strutture progettate secondo le Norme Tecniche per le Costruzioni* (RINTC),<sup>3</sup> has been developed by a joint working group formed between *Rete dei Laboratori Universitari di Ingegneria Sismica* (ReLUIS) and *Centro Europeo di Ricerca e Formazione in Ingegneria Sismica* (EUCENTRE), with the funding of *Presidenza del Consiglio dei Ministri – Dipartimento della Protezione Civile* (see, RINTC Workgroup 2017).

In the RINTC project, structures, belonging to a variety of typologies and configurations, were designed according to the current Italian code provisions in a number of sites at different hazard levels (Milan or MI, Caltanissetta or CL, Rome or RM, Naples or NA, and L'Aquila or AQ) and local site conditions (A and C according to EC8 classification). In Fig. 25.1 the considered sites are shown on the official Italian map of peak ground acceleration (PGA) with 475 years exceedance

---

<sup>3</sup>Project website's URL: [http://www.reluis.it/index.php?option=com\\_content&view=article&id=549&Itemid=198&lang=it](http://www.reluis.it/index.php?option=com_content&view=article&id=549&Itemid=198&lang=it)

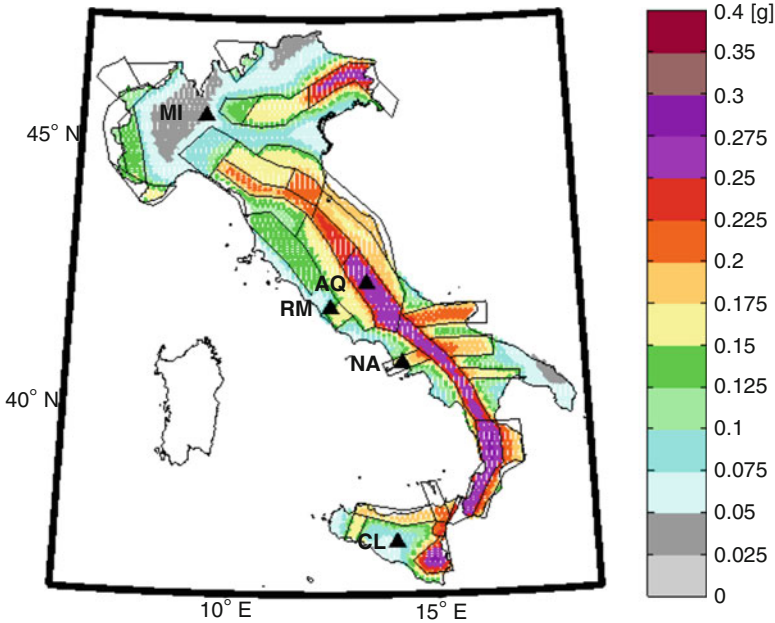


**Fig. 25.1** Location of construction sites considered in the RINTC project on the official seismic hazard map used for design (Stucchi et al. 2011) in terms of peak ground acceleration (PGA) with  $T_r = 475$  years on A-type EC8 soil site class

return period, which is the basis for design actions in NTC08. The map refers to A-type soil site class (see Stucchi et al. 2011 for details).

The structures have been designed for two code-defined limit states, that is, (a) *damage-control* and (b) *life-safety*.<sup>4</sup> The buildings are considered as *ordinary*, that is, the reference design actions at the construction site are those with return period equal to 50 years and 475 years for the former and latter limit states respectively. Elastic design action is represented by the *uniform hazard spectrum*, or UHS, for the site; i.e., the spectrum whose ordinates have all the return period of exceedance of interest (see also Sect. 25.8).<sup>5</sup>

The final results of the project are represented by the annual failure rates of the considered code-conforming structures. Failure is herein understood as the violation of two different performance levels: *convenient-to-repair damage* to non-structural elements (e.g., infills) and *global collapse* (i.e., life-safety-threatening structural failure). The risk is quantified in a state-of-the-art approach referring to performance-based earthquake engineering (PBEE; Cornell and Krawinkler 2000). In fact, for all the structures the failure rates are obtained by integrating probabilistic

<sup>4</sup>Base-isolated structures (to follow) are designed for *collapse-prevention*.

<sup>5</sup>In fact, in the Italian code spectra are UHS' approximated by via a simplified EC8-type functional form.

seismic structural vulnerability (i.e., *fragility*) and seismic hazard for the sites where the structures are located. To compute the failure rates, Eq. (25.1) is employed.

$$\lambda_f = \int_0^{+\infty} P[\text{failure}|IM = im] \cdot |d\lambda_{IM}(im)| \quad (25.1)$$

In the equation, IM indicates a ground motion intensity measure, while  $|d\lambda_{IM}(im)| = - [d\lambda_{IM}(im)/d(im)] \cdot d(im)$  is the differential of  $\lambda_{IM}(im)$ , or the *hazard curve*. It is the function providing the annual rate of earthquakes causing the exceedance of an IM threshold, indicated as *im*. The hazard curve is obtained from probabilistic seismic hazard analysis or PSHA (Cornell 1968); to follow.  $P[\text{failure}|IM = im]$  is the *fragility* function of the structure under analysis. It provides the probability of failure for  $IM = im$ ; i.e., for any arbitrary value of the ground motion intensity measure.

### 25.3 Structures and Modeling

The five structural types of buildings refer to standard modern constructions and are widely representative of residential or industrial structures in Italy. Design procedures refer as much as possible to common professional engineering practice. The considered cases as of the end of 2017 (the project is still ongoing) are:

1. cast-in-place reinforced concrete (RC) regular 3-, 6-, and 9-story residential moment-resisting-frame structures, designed via modal analysis (Camata et al. 2017), with the following configurations:
  - (a) bare-frames (BF);
  - (b) pilotis-frames (PF);
  - (c) infilled-frames (IF);
  - (d) (9-storey) with concrete structural walls (SW);
2. un-reinforced masonry (URM) 2- and 3-story residential buildings, with four different geometries, designed with the *simple building* and *linear* or *non-linear static analysis* approaches (Camilletti et al. 2017), with the following configurations
  - (a) regular;
  - (b) irregular;
3. pre-cast reinforced concrete (PRC) 1-story industrial buildings with two different plan geometries and two different heights (Ercolino et al. 2017), with the following configurations:
  - (a) without cladding panels;
  - (b) with cladding panels;

4. steel (S) 1-story industrial buildings (Scozzese et al. 2017) with two different plan geometries and two different heights, in analogy of configurations with respect to PRC:
  - (a) without cladding panels;
  - (b) with cladding panels;
5. base-isolated (BI) 6-story reinforced concrete residential buildings (Ponzo et al. 2017) with base isolation system made of:
  - (a) rubber bearings (HDRB);
  - (b) double-curvature friction pendulums (DCFP);
  - (c) hybrid (HDRB and sliders).

In the computation of failure rates, record-to-record variability of seismic response is the primary source of uncertainty; i.e., structural models are generally deterministic. However, for selected cases (indicated as ModUnc) of each typology, the uncertainty in structural modeling and in design has been accounted for following the approach described in Franchin et al. (2017); however, the effect of factors, such as quality of construction or design errors, was always neglected. Moreover, one selected case of 9-story RC with structural walls, includes explicit modeling of soil-structure-interaction (SSI).

Table 25.1 summarizes the case studies at the end of 2017. Note that, to reduce the effort, not all structures have been designed for all five sites, although most of

**Table 25.1** Designed and analyzed structures at the end of 2017

Type	Soil	MI	NA	AQ
RC	A	–	–	9-story (BF/PF/IF)
	C	3/6/9-story (BF/PF/IF)	3/6/9-story (BF/PF/IF)	3/6/9-story (BF/PF/IF)
		9-story SW	ModUnc	ModUnc
			9-story SW (also w/ SSI)	9-story SW
URM	A	2/3-story, regular/irregular	2/3-story, regular/irregular	2/3-story, regular ModUnc
	C	2/3-story, regular/irregular	2/3-story, regular/irregular	2/3-story, regular/irregular
PRC	A	1-story, 4 geometries	1-story, 4 geometries	1-story, 4 geometries
	C	1-story, 4 geometries	1-story, 4 geometries	1-story, 4 geometries
S	A	1-story, 4 geometries w/ and w/o panels	1-story, 4 geometries w/ and w/o panels	1-story, geometry 1/2/3/4 w/ and w/o panels
	C	1-story, 4 geometries w/ and w/o panels	1-story, 4 geometries w/ and w/o panels	1-story, 4 geometries w/ and w/o panels
BI	A	–	–	–
	C	–	6-story, HDRB/HDRB+slider	6-story, HDRB/HDRB w/ slider/DCFP (11 configurations) ModUnc

them have been designed for at least three sites reflecting low, moderate and high hazard levels (Milan, Naples, and L'Aquila, respectively)

## 25.4 Hazard

Equation (25.1) requires hazard curves to compute failure rates. The results of the probabilistic hazard study at the basis of NTC08 are available at <http://esse1-gis.mi.ingv.it/>. They are given in terms of hazard curves for 5%-damped (pseudo) spectral acceleration on A-type soil site class for eleven oscillation periods ( $T$ ) ranging from 0 s (PGA) to 2 s, computed for a grid featuring more than ten-thousands locations that covers the entire country. The curves are discretized at nine return periods, between 30 years and 2475 years. In the RINTC project the spectral (pseudo) acceleration,  $Sa$ , at the fundamental period of each structure ( $T_1$ ) is chosen as the ground motion intensity measure. Therefore, due to limitations in the soil type, oscillation periods for which  $Sa$  hazard is available, and return periods at which hazard is computed in the official study, the hazard curves at the sites of interest had to be re-computed for the scope of the RINTC project.

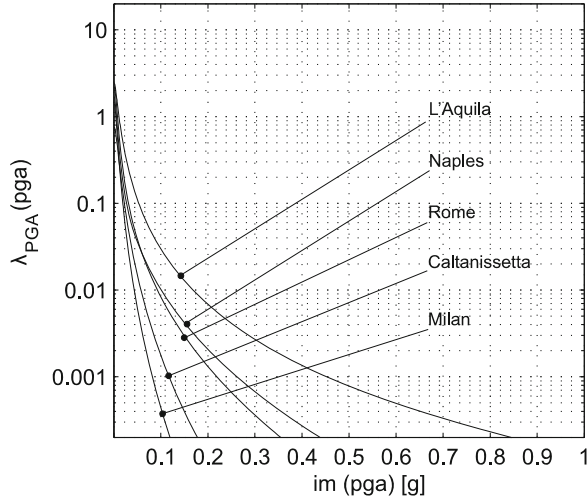
The hazard curves were calculated according to Eq. (25.2), where  $\nu_i$ ,  $i = \{1, 2, \dots, s\}$ , is the rate of earthquakes above a minimum magnitude for each of the  $s$  seismic sources affecting the site of interest. The term  $f_{M,R,i}(m,r)$  is the joint probability density function of magnitude ( $M$ ) and source-to-site distance ( $R$ ) for the  $i$ -th source, and  $P[IM > im | M = m, R = r]$  is the probability of exceeding the IM threshold conditional to  $\{M, R\}$ , provided by a ground motion prediction equation (GMPE).

$$\lambda_{IM}(im) = \sum_{i=1}^s \nu_i \cdot \iint_{M,R} P[IM > im | M = m, R = r] \cdot f_{M,R,i}(m,r) \cdot dm \cdot dr \quad (25.2)$$

If the calculation of Eq. (25.2) is repeated for all possible values of  $im$  within an interval of interest, one obtains the hazard curve providing  $\lambda_{IM}(im)$  as a function of  $im$ . As an illustration, Fig. 25.2 shows PGA hazard curves (for soil site class B according to EC8) for the five locations of the project. The curves were computed considering the *branch 921* of the logic tree described in Stucchi et al. (2011), which features the source characterization described in Meletti et al. (2008) and the GMPE of Ambraseys et al. (1996).<sup>6</sup> These models that constitute the core of the hazard model developed to produce the official seismic hazard map used for design in Italy, and were also used in the RINTC to determine the seismic risk according to Eq. (25.1).

<sup>6</sup>Note that assessing the performance of some structures required considering spectral accelerations at vibration periods not contemplated by the GMPE of Ambraseys et al. (1996), for these cases that of Akkar and Bommer (2010) was employed.

**Fig. 25.2** Example of hazard curves for the considered sites in terms of PGA on site class B (EC8 classification)



In addition, *disaggregation* of seismic hazard (e.g., Bazzurro and Cornell 1999), was carried out. It was required to perform hazard-consistent record selection required to run the non-linear dynamic analyses forming the basis of the risk assessment.

## 25.5 Fragility

Three-dimensional computer models were developed for all the designed structures with the aim of evaluating their seismic performance via non-linear dynamic analysis. The structural response measure or EDP (*engineering demand parameter*) considered was the maximum (in the two horizontal directions of the structure) demand over capacity ratio, expressed in terms of interstory drift angle or roof-drift angle. The main failure criterion for the assessment of global collapse was the drift corresponding to the 50% drop in base shear from the static push-over analysis (see RINTC Workgroup 2017). However, for some structural configurations some additional failure criteria were needed, for example, PRC required control of failure of connections, while base-isolated buildings required specific criteria for failure of the isolation system. For damage to non-structural elements, multiple failure criteria considering the extent of damage over the building, were considered.

All models are lumped-plasticity, except for the industrial steel building cases that were modeled using distributed plasticity elements. All structures are analyzed with OPENSEES (Mazzoni et al. 2006) apart from the masonry structures that are analyzed using TREMURI (Lagomarsino et al. 2013).

It was mentioned that  $P[\text{failure}|IM = im]$  as a function of  $im$  is the fragility function of the structure. In this study, for each considered structure, the fragility curve was computed via non-linear dynamic analysis using Eq. (25.3). To this aim,

the domain of IM, that is  $Sa(T_1)$ , has been discretized to ten values, corresponding to the following return periods from the hazard curve of interest:  $T_r = \{10, 50, 100, 250, 500, 1000, 2500, 5000, 10000, 100000\}$  years.

$$P[\text{failure}|IM = im_i] = \left\{ 1 - \Phi \left[ \frac{\log(edp_f) - \mu_{\log(EDP|IM=im_i)}}{\sigma_{\log(EDP|IM=im_i)}} \right] \right\} \cdot \left( 1 - \frac{N_{col,IM=im_i}}{N_{tot,IM=im_i}} \right) + \frac{N_{col,IM=im_i}}{N_{tot,IM=im_i}} \quad (25.3)$$

In the equation,  $edp_f$  indicates structural seismic capacity for the performance level of interest;  $\left\{ \mu_{\log(EDP|IM=im_i)}, \sigma_{\log(EDP|IM=im_i)} \right\}$  are the mean and standard deviation of the logs of EDP when  $IM = im_i$ ,  $i = \{1, \dots, 10\}$ ;  $\Phi(\cdot)$  is the cumulative Gaussian distribution function;  $N_{col,IM=im_i}$  is the number of collapse cases (i.e., those reaching global instability according to the terminology in Shome and Cornell 2000); and  $N_{tot,IM=im_i}$  is the number of ground motion records with  $IM = im_i$ .

The method to probabilistically evaluate structural response, and then fragility, was the *multi-stripe* nonlinear dynamic analysis (e.g., Jalayer 2003). To select the ground motion records to be used as input for dynamic analysis, the hazard-consistent *conditional spectrum* (CS) approach (e.g., Lin et al. 2013), has been considered. Ground motion record sets selected for each CS are consistent with the earthquake scenarios (expressed in terms of magnitude and source-to-site distance) that contributed the most to  $Sa(T_1) = im_i$  according to disaggregation of site hazard. Because the scenarios controlling the hazard, in general, change with the specific value of  $Sa(T_1)$  considered, different sets of records were selected for each hazard level (see Iervolino et al. 2017, for some details). All the analyses neglected, so far, the vertical components of ground motion as specific analyses show no need to take them into account.

## 25.6 Trend of Failure Rates

Equation (25.1) can be used for the computation of failure rates only for the values of  $\lambda_{IM}(im)$  provided by hazard analysis. The latter, has a limit at  $1/T_r = 10^{-5}$  [event/year]; in fact, no  $Sa(T_1)$  values for return periods longer than  $T_r = 10^5$  years were calculated, to avoid large hazard extrapolations. Therefore, it has been conservatively assumed that ground motions with an IM larger than that corresponding to  $T_r = 10^5$  years, cause failure with certainty. This means that the failure rate has been approximated in excess by Eq. (25.4).

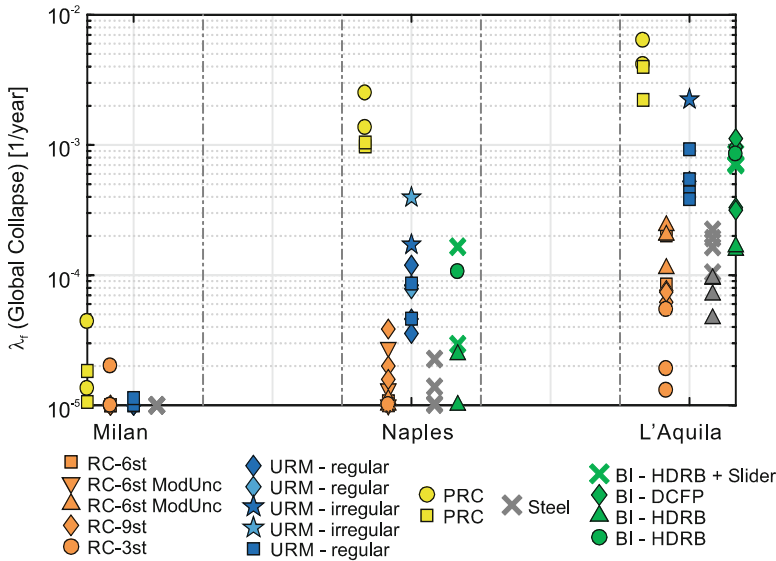


**Fig. 25.3** Failure rates for global collapse (soil site class C) at three of the considered sites in ascending order of hazard. (Figure adapted from Iervolino et al. 2017)

$$\lambda_f = \int_0^{im_{T_r=10^5}} P[failure|IM = im] \cdot |d\lambda_{IM}(im)| + 10^{-5} \tag{25.4}$$

In the equation,  $im_{T_r=10^5}$  indicates the last available  $im$ -value for which a return period of exceedance has been calculated. Consequently, in those cases when the first part of the integral is negligible with respect to  $10^{-5}$ , then Eq. (25.4) only allows to state that the annual failure rate is lower than  $10^{-5}$ .

Figures 25.3 reports the global collapse failure rates, as of the end of 2016, for soil site class C at three of the considered sites. These results, although not final, indicate the following:

1. as a general trend, the collapse failure rates generally tend to increase with the site hazard, independent of the structural type considered (likely due to over-strength imposed at moderate-to-low hazard sites by, for example, minimum design requirements; see also Suzuki et al. 2017);
2. the failure rates tend not to be uniform among different structural types designed for the same site hazard;
3. in some cases, the collapse failure rates are so low that only an upper bound to the actual failure rate can be provided; i.e.,  $\lambda_f \leq 10^{-5}$ ; however, in other cases it is comparable to (or larger than) the annual rate of exceedance of the design seismic intensity; e.g.,  $1/475 = 0.0021$ .

Although these general trends clearly emerge from the last three years of the RINTC project, it is emphasized that it is still ongoing and several of these results (and other not shown here) are undergoing verification and investigation towards

consolidation. Caution should be applied in using all results presented. For example, the critically-high risk exhibited by some PRC structures are likely due to some design and modeling options of beam-to-column connections and, therefore, are not definitive. Similarly, the comparatively high collapse failure rates of base-isolated structures seem due to their more controlled behavior during design and the lower margin of safety with respect to collapse beyond the maximum design displacement; conversely, base-isolated structures show comparatively lower rates of onset of damage to non-structural elements (not shown here).

## 25.7 The Nature of Uniform-Hazard Design Spectra

It has been discussed with what frequency (annual rate) failure is expected for code-conforming structures; in this part of the paper it is analyzed which earthquakes erode the safety margins that depend on the elastic design seismic actions (Iervolino and Giorgio 2017).

The latest version of the Italian earthquake catalogue (CPTI15; <http://emidius.mi.ingv.it/CPTI15-DBMI15/>), assigns moment magnitude larger than six to thirteen earthquakes in the 1915–2014 period, which translates to an average of one event every eight years in the past century. During the last decade, among the main (i.e., severely damaging) seismic sequences for the country, one counts that of L’Aquila (2009), that of Emilia (2012) and that of central Italy 2016–2017 (the latter not included in CPTI15), whose largest (moment) magnitude earthquakes were 6.3, 6.1 and 6.5, respectively. In the same period of these events, NTC08 went into effect, which, as mentioned, prescribe seismic design actions determined on a probabilistic basis by means of the uniform hazard spectra or UHS’ that were also used for design in the RINTC project.

The recent seismic events provided an unprecedented level of instrumental recordings, for the country (see for example Luzi et al. 2017). These data allow a comparison of actually-observed seismic actions with their code-prescribed counterparts used for designing new structures. Said comparison has repeatedly shown registered seismic actions, in the epicentral areas, systematically exceeding design spectra, which, in turn, vamped a debate on whether the design actions were incorrectly evaluated. The objective herein is to demonstrate that such exceedance is well expected based on the nature of UHS’. Observed exceedances cannot be considered sufficient to claim that the code-mandated seismic actions underestimate the seismic hazard. On the contrary, they are a foreseeable consequence of the philosophy that underlies definition of seismic actions in the code, when it is based on probabilistic seismic hazard. Consequently, it is also shown that UHS represent design action likely exceeded in the epicentral areas of earthquakes occurring relatively frequently in Italy. Thus, in these events, safety is mostly entrusted to the safety margins beyond the elastic design spectrum.

To prove the proposition, the starting point is discussing the seismic actions observed during the 2009 L’Aquila earthquake (e.g., Chioccarelli et al. 2009).

**Fig. 25.4** Response spectra of horizontal ground motion recorded at L’Aquila (AQV station) during the 6.3 moment-magnitude earthquake of 2009 and code spectrum for  $T_r = 475$  years (soil site class is B according to the EC8 classification, as reported for AQV the Italian Accelerometric Archive; <http://itaca.mi.ingv.it/>)

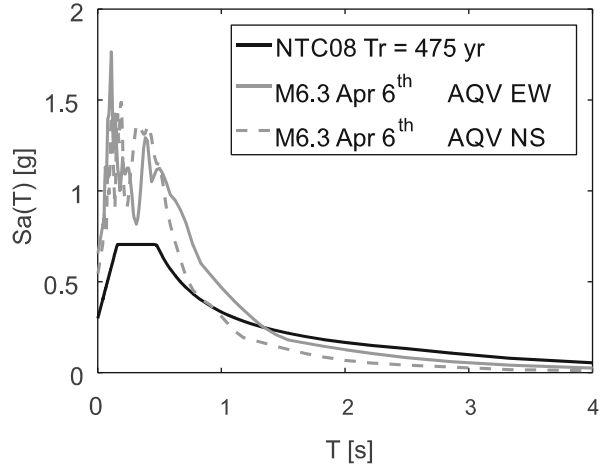


Figure 25.4 shows the spectra of the horizontal components of seismic ground motion recorded in L’Aquila (AQV monitoring station of the *Rete Accelerometrica Nazionale* managed by the Italian *Dipartimento della Protezione Civile*; <http://ran.protezionecivile.it>) during the considered earthquake. The same figure also shows the NTC08 spectrum to be used for life-safety limit-state design of ordinary construction at the AQV site (i.e., the UHS with 475 years return period of exceedance), this is the same as the one used in RINTC except for soil site class, which matches the one of the recording station, for comparison purposes. One notices that the design actions have been greatly exceeded over a relatively wide interval of natural vibration periods, including the  $Sa(T = 1\text{ s})$  ordinate, which will be analyzed in the following. It will be shown forthwith that this is neither strange nor an indicator of deficiency of the code spectra themselves, but it is instead a predictable consequence of the nature of code spectra.

### 25.8 Scenario Contributions to Design Hazard

As already mentioned, the elastic design spectra of the Italian code are uniform hazard spectra. Such spectra are computed, for a given construction site, by means of probabilistic seismic hazard analysis described by Eq. (25.2) above.

It is now useful, for the purposes of this study, to rewrite the hazard integral as in Eq. (25.5), considering, for example, the  $Sa(T = 1\text{ s})$  as the IM.

$$\lambda_{Sa(T=1s)}(sa) = \iint_{M,R} P[Sa(T = 1\text{ s}) > sa | M = m, R = r] \cdot \nu_{M=m,R=r} \cdot dm \cdot dr \tag{25.5}$$

In the equation,  $\nu_{M=m, R=r} \cdot dm \cdot dr = \sum_{i=1}^S \nu_i \cdot f_{M,R,i}(m, r) \cdot dm \cdot dr$  represents the rate of earthquakes of magnitude  $(m, m + dm)$  that originate at a distance equal  $(r, r + dr)$  (accounting for all considered seismic sources).

The hazard integral can be further compacted as in Eq. (25.6), where  $\lambda_{Sa(T=1s) > sa, M=m, R=r} \cdot dm \cdot dr = P[ Sa(T=1s) > sa | M=m, R=r ] \cdot \nu_{M=m, R=r} \cdot dm \cdot dr$  is the rate of earthquakes of magnitude  $(m, m + dm)$  that originate at a distance  $(r, r + dr)$ , and cause exceedance of the intensity threshold,  $sa$ .

$$\lambda_{Sa(T=1s)}(sa) = \iint_{M,R} \lambda_{Sa(T=1s) > sa, M=m, R=r} \cdot dm \cdot dr \tag{25.6}$$

$\lambda_{Sa(T=1s) > sa, M=m, R=r} \cdot dm \cdot dr$  is the contribution to hazard of the earthquake scenario with magnitude  $(m, m + dm)$  at distance  $(r, r + dr)$  from the site. (In the following, for computation/representation purposes,  $dm$  and  $dr$  are replaced by small, yet finite, magnitude and distance bins,  $\Delta m$  and  $\Delta r$ , respectively.)

Focusing, for example, attention on  $Sa(T=1s)$  with  $\lambda_{Sa(T=1s)} = 0.0021$  (i.e., the  $Sa(T=1s)$  value with  $T_r = 475$  years at the site), let us call this value  $sa_{T_r=475}$ , it is evident from Eq. (25.6) that none of the aforementioned single contributions may exceed this value; i.e.,  $\lambda_{Sa(T=1s) > sa, M=m, R=r} \cdot \Delta m \cdot \Delta r \leq 0.0021, \forall \{m, r\}$ . Because the lowest magnitude earthquakes are, typically, more frequent than higher magnitudes, this limitation is met in a way that when the former events occur, they have a low probability of exceeding the acceleration threshold that corresponds to that rate. Conversely, the latter events, having low recurrence rate can have high exceedance probability; i.e.,  $P[ Sa(T=1s) > sa | M=m, R=r ]$  can approach one.

To better illustrate the point, Fig. 25.5 provides a discretized representation, in terms of magnitude-distance bins, of the individual contributions of magnitude and distance pairs to  $sa_{T_r=475}$  at L'Aquila. Such a representation is obtained using the same hazard component models described in Sect. 25.4 and used for the RINTC project, which yielded  $sa_{T_r=475} = 0.27g$  on EC8 soil site class B.

Figure 25.5 (bottom) provides the rates  $\lambda_{Sa(T=1s) > sa, M=m, R=r} \cdot \Delta m \cdot \Delta r$  [1/year], that is, for each  $\{M, R\}$  bin (i.e., a scenario), the average number of earthquakes per year causing exceedance of  $sa_{T_r=475} = 0.27g$  (by definition, the sum of these rates over all the bins is equal to 0.0021).<sup>7</sup> Fig. 25.5 (top-left) gives the rates of occurrence of earthquakes corresponding to each bin; i.e.,  $\nu_{M=m, R=r} \cdot \Delta m \cdot \Delta r$  [1/year]. Finally, Fig. 25.5 (top-right) provides the probability that earthquakes corresponding to each magnitude-distance scenario cause exceedance of 0.27 g; i.e.,  $P[ Sa(T=1s) > sa_{T_r=475} | M=m, R=r ]$ . The product of values in Fig. 25.5 (top-left) and Fig. 25.5 (top-right), corresponding to the same  $\{M, R\}$  bin, provides the value in Fig. 25.5 (bottom) for that bin; see Eq. (25.5).

The rates of occurrence in Fig. 25.5 (top), rapidly decrease with increasing magnitude, independently of distance, as expected. Looking at the dependence of  $\nu_{M=m, R=r} \cdot \Delta m \cdot \Delta r$  on source-to-site distance, it appears that the rates tend to

<sup>7</sup>Note that the table factually represents the distribution of magnitude and distance one obtains from hazard disaggregation multiplied by 0.0021.

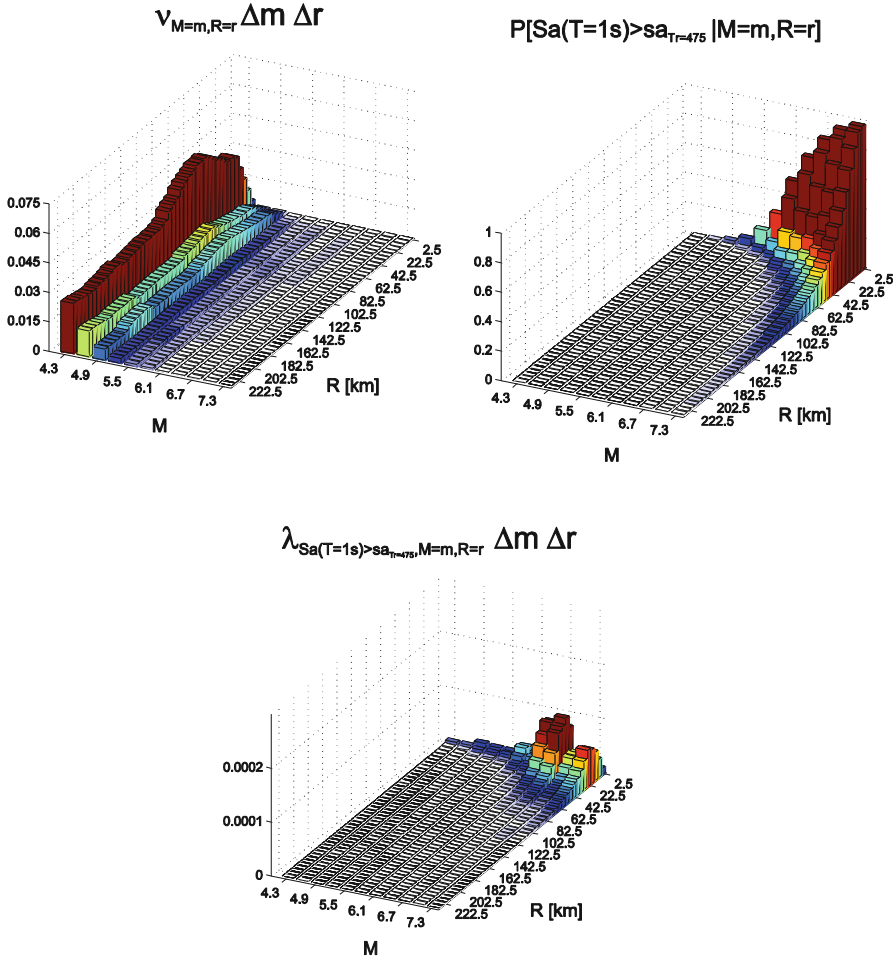


**Fig. 25.5** Scenario representation of the hazard at L’Aquila in terms of  $Sa(T = 1s)$  with exceedance return period equal to 475 years. The top-left panel reports the rates of occurrence [1/year] of magnitude-distance bins; the top-right panel provides the probability of exceedance, of  $sa_{T_r=475}$ , for each bin; the bottom is panel the product of the previous two bin-by-bin. Summing-up bars in the bottom panel provides  $0.0021 = 1/475$  and corresponds to the integral of Eq. (25.6).

decrease with distance approaching to zero, because relatively smaller portions of the source zones fall in a circle/ring with center in the site of interest and smaller radius. Consequently, there is a large number of bins with small-to-very-small occurrence rate (i.e., white areas in the figure), they correspond to large magnitudes at all distances, or moderate-to-large magnitudes at small distance.

Figure 25.5 (center) provides the effect of the magnitude-distance scenarios in terms of probability of exceeding  $sa_{T_r=475}$ . Because such a probability increases with increasing magnitude and decreasing distance as indicated by GMPEs, it can be seen

that several bins with low rate in the top panel can have very large exceedance probability, if they actually occur, that approaches one in some cases. In particular, the exceedance probability, conditional to  $\{M, R\}$ , starts to be significant for  $M \geq 6$ ,  $R \leq 5\text{km}$ , but it is large up to  $R \approx 60\text{km}$  for magnitudes larger than seven.

As mentioned, Fig. 25.5 (bottom) reports the hazard contributions of magnitude-distance scenarios, weighing the exceedance probability of each scenario by its occurrence rate:  $\lambda_{Sa(T=1s) > sa, M=m, R=r} = P[Sa(T=1s) > sa | M=m, R=r] \cdot \nu_{M=m, R=r}$ . It appears from the figure that the  $\{M, R\}$  pairs giving the largest contributions are, in general, close earthquakes, because of their large  $P[Sa(T=1s) > sa | M=m, R=r]$ . However, the largest values of  $\lambda_{Sa(T=1s) > sa, M=m, R=r} \cdot \Delta m \cdot \Delta r$  do not correspond to the largest magnitude occurring at the smallest distance, because these are very rare events; i.e., with comparatively small  $\nu_{M=m, R=r} \cdot \Delta m \cdot \Delta r$ .

In fact, among the close-by earthquakes the most significant exceedance rates are given by smaller magnitudes. These events are more frequently occurring close to the site than extreme magnitudes, yet the probability of exceeding the threshold for some of them is not small at all, as demonstrated in the next section.

## 25.9 Close Earthquakes

As expected, close-by earthquakes give the largest contribution to hazard. In fact, summing up the values of the bars from  $\{M, R\}$  bins up to  $R \leq 50\text{km}$  in Fig. 25.5 (bottom) one obtains 0.019, which means that the earthquakes occurring within this distance account for 90% of the contributions to  $Sa(T=1s)$  hazard with exceedance return period  $T_r = 475$  years in L'Aquila. This is a common situation when the site is within a seismic source zone that dominates the hazard (see Iervolino et al. 2011).

Focusing exclusively on the contributions of the earthquakes occurring within 50 km, it can be seen that there are different magnitudes with similar contributions. For example, an earthquake of magnitude  $M \in (5.05, 5.35)$  at a distance between  $0\text{km} \leq R < 5\text{km}$  has  $\lambda_{Sa(T=1s) > sa, M=m, R=r} \cdot \Delta m \cdot \Delta r$  equal to about  $1.2\text{E-}5$  [1/year], which is about the same of an earthquake of magnitude  $M \in (6.85, 7.15)$  at distance  $0\text{km} \leq R < 5\text{km}$ . However, this equivalent contribution to hazard arises from very different occurrence rates and conditional exceedance probabilities, as it can be seen in Table 25.2, where the values from the three panels Fig. 25.5 are given for the two scenarios.

Analyzing Table 25.2 is crucial in demonstrating the initial proposition of this part of the paper. Despite the same threshold exceedance rate, the two scenarios are very different in rarity, as expected. With the lower magnitude being about fifteen times more frequent than the larger. Conversely, when an earthquake  $M \approx 5.2$  occurs close to the site, it has 6% probability of exceeding the  $Sa(T=1s)$  ordinate of the  $T_r = 475$  years UHS for L'Aquila; i.e., in case of occurrence there is 0.94% chance that the UHS is not exceeded at the  $T=1s$  ordinate. Conversely, if L'Aquila were close to an  $M \approx 7$  event, then the probability of exceeding the threshold would be larger than 90%. It immediately follows from this reasoning that the UHS is hard to

**Table 25.2** Two scenarios with comparable contributions to hazard, but very different frequency of occurrence and probability of exceeding the design  $Sa(T = 1s)$  in L’Aquila in case of occurrence

	$5.05 \leq M < 5.35,$ $0 \leq R < 5$	$6.85 \leq M < 5.15,$ $0 \leq R < 5$
$\nu_{R=r, M=m} \cdot \Delta m \cdot \Delta r$ [1/year]	2.0E-4	1.3E-5
$P[Sa(T = 1s) > sa_{T_r=475}   M = m, R = r]$	6E-2	9E-1
$\lambda_{Sa(T=1s) > sa_{T_r=475}, M=m, R=r} \cdot \Delta m \cdot \Delta r$ [1/year]	1.2E-5	1.2E-5

be exceeded only by distant earthquakes or by the relatively more frequent among close earthquakes. On the other hand, it is very likely to almost certain, depending on the magnitude (see Fig. 25.5, center), that it is going to be exceeded by the more rare among close-by earthquakes. Therefore, the UHS may not represent a high threshold in the case of occurrence of this kind of earthquakes.

It must be underlined that this reasoning does not question that the ordinates of the UHS for the site are exceeded, as intended, on average once every 475 years. However, this exceedance return period, for the rarest earthquakes, is warranted by the fact that their occurrence close to the site is unlikely. On the other hand, when such earthquakes do occur near a given site, the exceedance of design actions can be probable-to-very-probable, depending on the considered scenario.

Similar reasoning can be applied to any other spectral ordinate and/or return period, although the range of scenarios to which it applies is expected to change in the very same way disaggregation depends on the spectral ordinate or return period under consideration.

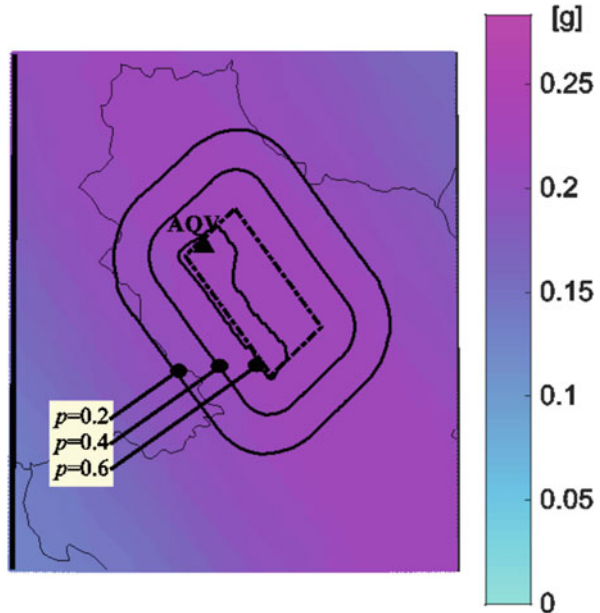
## 25.10 What to Expect for a Magnitude 6.3 Event

In the light of all that was shown above, one may now return to examine what happened at AQV during the mainshock of the L’Aquila 2009 earthquake.

AQV was at close distance to the epicenter (zero in terms of Joyner and Boore 1981, distance, which is the distance from the surface projection of the earthquake rupture), then it was somewhat likely to observe exceedance of the  $T_r = 475$  years UHS at that site. In fact, according to the GMPE of Ambraseys et al. (1996), for an earthquake of magnitude 6.3 at 0 km,  $P[Sa(T = 1s) > 0.27g | M = 6.3, R = 0] > 0.6$  on soil site class B (see Fig. 25.5, center). Therefore, first, exceedance of the  $T_r = 475$  years  $Sa(T = 1s)$ , observed in Fig. 25.4, is in accord with the models underlying hazard analysis. Second, the earthquakes exceeding the UHS with very high probability are not necessarily of especially high magnitude (see Fig. 25.5 center).

As a matter of fact, this discussion could be extended for the entire epicentral area of the earthquake. In order to understand which are the locations where exceedance of design actions ought to have been avoided, one should examine Fig. 25.6. First thing shown on that figure is the surface projection of the rupture that caused

**Fig. 25.6** Design  $S_a$  ( $T = 1$ s) (i.e., those from Fig. 25.1 with 475 years exceedance return period) for the area hit by the April 6th 2009 (moment magnitude 6.3) L'Aquila earthquake and equal probability contours for their exceedance due to an earthquake with the same magnitude and localization as the one that actually occurred



the earthquake (dash-dot line) and the administrative limits of the area’s municipalities (thin black lines). On the same figure, the  $sa_{Tr = 475}$  values for the area, from the analysis described in Stucchi et al. 2011,<sup>8</sup> are shown as colored contours. The black iso-probability delimit areas exhibiting various probabilities,  $P[Sa(T = 1s) > sa_{Tr=475} | M = m, R = r]$ , of observing the exceedance of the code-mandated design actions depicted in the underlying colored contours. The probabilities were calculated using the GMPE of Ambraseys et al. (1996), the same employed when determining the code design actions of the underlying colored map, so that the calculations are consistent.

One notes that, in a relatively wide area on/around the source, the exceedance of design  $Sa(T = 1s)$  was likely (e.g., larger than 50%) for an earthquake of the magnitude and location as those occurred on April 6th 2009. As argued for the individual case of AQV, this is by no means contradicting the hazard map but it is rather an intrinsic characteristic thereof. On the other hand, the probability of exceeding the seismic actions rapidly decreases as one moves farther away from the rupture.

<sup>8</sup>Consistent with Figure 25.1, the design  $Sa(T = 1s)$  map refers to type A EC8 site class.

## 25.11 Conclusions

This article presented some arguments about when and where damages are expected for code-conforming structures. The developed studies refer to Italy, however they might have an international appeal as Italy is at the state of the art of seismic codes internationally and its design norms have extensive similarities with Eurocode 8.

From the description of the RINTC project, a large research effort towards the assessment of seismic risk for different structural typologies, it seems to mainly emerge that the seismic risk for structures designed with nominally equivalent design actions is increasing with the hazard at the site; thus, more risky structures are designed for the most hazardous sites, although design actions at the different sites refer to the same return periods. Thus, design based on the same hazard does not lead to the same risk for the designed structures.

From a closer look to the nature of uniform hazard spectra (on the basis of which design actions are determined in the Italian code) it emerges that design elastic actions are likely-to-very-likely going to be exceeded in the case of moderate-to-high magnitude earthquakes, were they to occur close to the site. In other words, the UHS', generally, represent intensity thresholds hard to surpass by far-away earthquakes or by those of lower magnitude among those close-by. Conversely, they do not represent conservative thresholds for earthquakes relatively rare in occurrence and near the site. This is well expected, and does not represent a reason to blame the way that probabilistic spectra are determined. However, the conclusion for code-conforming constructions is that safety against violation of the design limit states in the epicentral area of earthquakes, which are observed relatively frequently all-over a country such as Italy, is entrusted to safety margins beyond the elastic design spectrum.

**Acknowledgments** The study was developed between 2015 and 2017 in the framework the *Rete dei Laboratori Universitari di Ingegneria Sismica* activities funded by *Presidenza del Consiglio dei Ministri – Dipartimento della Protezione Civile* (2014–2018 program). The help from Andrea Spillatura (IUSS, Pavia, Italy) and Pasquale Cito (University of Naples Federico II, Italy) is also gratefully acknowledged.

## References

- Akkar S, Bommer JJ (2010) Empirical equations for the prediction of PGA, PGV, and spectral accelerations in Europe, the Mediterranean region, and the Middle East. *Seismol Res Lett* 81:195–206
- Ambraseys NN, Simpson KU, Bommer JJ (1996) Prediction of horizontal response spectra in Europe. *Earthq Eng Struct Dyn* 25:371–400
- Bazzurro P, Cornell CA (1999) Disaggregation of seismic hazard. *Bull Seismol Soc Am* 89:501–520
- Camata G, Celano F, De Risi MT et al (2017) RINTC project: nonlinear dynamic analyses of Italian code-conforming reinforced concrete buildings for risk of collapse assessment. In Papadrakakis M, Fragiadakis M (eds) *Proceedings of COMPDYN 2017 – 6th ECCOMAS*

- thematic conference on computational methods in structural dynamics and earth-quake engineering, Rhodes (GR) 2017
- Camilletti D, Cattari S, Lagomarsino S et al (2017) RINTC project: Nonlinear dynamic analyses of Italian code-conforming URM buildings for collapse risk assessment. In Papadrakakis M, Fragiadakis M (eds) Proceedings of COMPDYN 2017 – 6th ECCOMAS thematic conference on computational methods in structural dynamics and earth-quake engineering, Rhodes (GR) 2017
- CEN, European Committee for Standardisation (2004) Eurocode 8: design provisions for earthquake resistance of structures, Part 1.1: general rules, seismic actions and rules for buildings, EN 1998-1
- Chioccarelli E, De Luca F, Iervolino I (2009) Preliminary study on L'Aquila earthquake ground motion records V5.2. Available at <http://www.reluis.it/>. Last accessed December 2017
- Cornell CA (1968) Engineering seismic risk analysis. *Bull Seismol Soc Am* 58:1583–1606
- Cornell CA, Krawinkler H (2000) Progress and challenges in seismic performance assessment. *PEER Center News* 3:1–3
- CS.LL.PP (2008) DM 14 gennaio, Norme tecniche per le costruzioni *Gazzetta Ufficiale della Repubblica Italiana* 29 (in Italian)
- Ecolino M, Cimmino M, Magliulo G et al (2017) RINTC project: nonlinear analyses of Italian code conforming precast R/C industrial buildings for risk of collapse assessment. In Papadrakakis M, Fragiadakis M (eds) Proceedings of COMPDYN 2017 – 6th ECCOMAS thematic conference on computational methods in structural dynamics and earth-quake engineering, Rhodes (GR) 2017
- Franchin P, Mollaioli F, Noto F (2017) RINTC project: influence of structure-related uncertainties on the risk of collapse of Italian code-conforming reinforced concrete buildings. In Papadrakakis M, Fragiadakis M (eds) Proceedings of COMPDYN 2017 – 6th ECCOMAS thematic conference on computational methods in structural dynamics and earth-quake engineering, Rhodes (GR) 2017
- Iervolino I, Giorgio M (2017) Regional exceedance frequency of uniform hazard spectra (Which earthquakes do design spectra protect against?) (In review)
- Iervolino I, Chioccarelli E, Convertito V (2011) Engineering design earthquakes from multimodal hazard disaggregation. *Soil Dyn Earthq Eng* 31:1212–1231
- Iervolino I, Spillatura A, Bazzurro P (2017) RINTC project: assessing the (implicit) seismic risk of code-conforming structures in Italy. In Papadrakakis M, Fragiadakis M (eds) Proceedings of COMPDYN 2017 – 6th ECCOMAS thematic conference on computational methods in structural dynamics and earth-quake engineering, Rhodes (GR) 2017
- Jalayer F (2003) Direct probabilistic seismic analysis: implementing non-linear dynamic assessments. Thesis, Stanford University
- Joyner WB, Boore DM (1981) Peak horizontal acceleration and velocity from strongmotion records including records from the 1979 Imperial Valley, California, Earthquake. *Bull Seismol Soc Am* 71:2011–2038
- Lagomarsino S, Penna A, Galasco A et al (2013) TREMURI program: an equivalent frame model for the nonlinear seismic analysis of masonry buildings. *Eng Struct* 56:1787–1799
- Lin TG, Haselton CB, Baker JW (2013) Conditional spectrum-based ground motion selection. Part I: hazard consistency for risk-based assessments. *Earthq Eng Struct Dyn* 42:1847–1865
- Luzi L, Pacor F, Puglia R et al (2017) The Central Italy seismic sequence between august and December 2016: analysis of strong-motion observations. *Seismol Res Lett* 88:1219–1231
- Mazzoni S, McKenna F, Scott MH et al (2006) OpenSees command language manual. Available at <http://opensees.berkeley.edu/>. Last accessed December 2017
- Meletti C, Galadini F, Valensise G et al (2008) A seismic source zone model for the seismic hazard assessment of the Italian territory. *Tectonophysics* 450:85–108
- Ponzo FC, Cardone D, Dall'Asta A et al (2017) RINTC project: nonlinear analyses of Italian code-conforming base-isolated buildings for risk of collapse assessment. In Papadrakakis M, Fragiadakis M (eds) Proceedings of COMPDYN 2017 – 6th ECCOMAS thematic conference

- on computational methods in structural dynamics and earth-quake engineering, Rhodes (GR) 2017
- RINTC Workgroup (2017) Results of the 2015–2016 RINTC project. Available at <http://www.reluis.it/>. Last accessed December 2017
- Scozzese F, Terracciano G, Zona A et al (2017) RINTC project: nonlinear dynamic analyses of Italian code-conforming steel single-story buildings for collapse risk assessment. In Papadrakakis M, Fragiadakis M (eds) Proceedings of COMPDYN 2017 – 6th ECCOMAS thematic conference on computational methods in structural dynamics and earth-quake engineering, Rhodes (GR) 2017
- Shome N, Cornell CA (2000) Structural seismic demand analysis: consideration of “collapse”. In PMC2000 – 8th ASCE Specialty Conference on Probabilistic Mechanics and Structural Reliability. University of Notre Dame, South Bend, Indiana, 24–26 July 2000
- Stucchi M, Meletti C, Montaldo V et al (2011) Seismic hazard assessment (2003–2009) for the Italian building code. *Bull Seismol Soc Am* 101:1885–1911
- Suzuki A, Baltzopoulos G, Iervolino I et al (2017) A look at the seismic risk of Italian code-conforming RC buildings. In: Proceedings of 16th Europeasn conference on earthquake engineering, Thessaloniki (GR), 18–21 June 2018